Cascade Extended State Observer for ADRC Applications under Measurement Noise

Krzysztof Łakomy, Rafal Madonski

arXiv:2004.01483v1 [eess.SY] 3 Apr 2020

***Abstract*—The extended state observer (ESO) plays an important role in the design of feedback control for nonlinear systems. It is also the key component in any active disturbance rejection control (ADRC) scheme. However, its high-gain nature creates a challenge in engineering practice in cases where the output measurement is corrupted by non-negligible, high-frequency noise. The presence of measurement noise puts a constraint on how high the observer gain can be, which forces a trade-off between fast convergence of state estimates and quality of control task realization. In this brief, a new approach is proposed to redesign the observer part in order to improve its performance in the presence of noise. In particular, an unique cascade combination of ESOs is developed, which is capable of fast and accurate signals reconstruction, while avoiding over-amplification of the measurement noise. The design stage of cascade ESO is followed by the theoretical analysis and the simulation validation showing improvement over conventional solution in terms of noise attenuation.**

***Index Terms*—High-gain observers, Noise filtering, Active disturbance rejection control, ADRC, Extended state observer, ESO**

I. Introduction

A common strategy in the class of active disturbance rejection control (ADRC [1], [2]) techniques for extracting otherwise unavailable information about the governed system is to use an extended state observer (ESO [3]). It simultaneously provides information about the missing state variables (required for controller synthesis) as well as the lumped disturbances/uncertainties (also denoted as *total disturbance* [4]). Successful deployments of ADRC in various control areas have been well documented (see recent examples [5], [6], [7]).

To a large extent, the performance of any ADRC scheme relies on the speed and accuracy of the ESO. It is well-known that high-gain observers (including ESO) are robust against model uncertainty and disturbances. However, the theory of observers also reveals the existence of a trade-off between speed/accuracy of state reconstruction and sensitivity to high-frequency measurement noise [8]. This problem is still an active research topic with different solutions proposed to date to attenuate the effects of measurement noise. They mainly address the problem by: employing nonlinear ([3], [9]) or adaptive techniques ([10], [11], [12]), redesigning the local behavior by combining different observers ([13], [14], [15], [16]), employing low-power structures ([17], [18]), increasing the observer order with integral terms [19], adding special saturation functions ([20], [21]), or modifying standard low-pass filters [22], [23].

Motivated by this practically important problem, in this brief, a new paradigm to redesign high-gain observers is proposed in order to improve their performance in the presence of measurement noise. It directly addresses the limitation posed by the trade-off between speed/accuracy of state estimation and noise sensitivity. The principle behind the proposed approach is based on decomposition of the unknown total disturbance into a predefined number of parts, each representing certain signal frequency range, and reconstruction of the decomposed parts with a set of cascaded observers. In contrast to a standard, single-observer ADRC, the introduced multi-observer topology allows to use higher observer bandwidths for reconstructing signals with smaller sensor noise impact. Hence, the contribution of this work is a proposition of the new cascade ESO topology, which is capable of providing fast and accurate estimates while avoiding over-amplification of the sensor noise. To best of our knowledge, such design is presented for the first time in the context of current literature.

Notation. Throughout this paper, we use $\mathbb{R}$ as a set of real numbers, $\mathbb{R}_+ = \{x \in \mathbb{R} : x \geq 0\}$ as a set of positive real numbers, $\mathbb{Z}$ as a set of integers, while $\mathbf{0}$ and $\boldsymbol{I}$ represent zero and identity matrices of the appropriate order, respectively. Relation $\boldsymbol{A} \succ 0$ means that $\boldsymbol{A}$ is positive-definite, $\|\boldsymbol{x}\|$ corresponds to the Euclidean norm of the vector $\boldsymbol{x}$, $\|\boldsymbol{A}\|$ is a matrix norm defined as $\|\boldsymbol{A}\| \triangleq \sup\{\|\boldsymbol{A}\boldsymbol{x}\| : \boldsymbol{x} \in \mathbb{R}^n \text{ and } \|\boldsymbol{x}\| = 1\}$, while $\lambda_{\min}(\boldsymbol{A})$ and $\lambda_{\max}(\boldsymbol{A})$ correspond to the minimal and maximal eigenvalues of matrix $\boldsymbol{A}$. Set $\mathcal{C}^1$ represents a class of Lipschitz continuous functions, while $\mathcal{K}$ is a class of strictly increasing functions with the zero-value at the origin.

II. Standard ESO design

Before the proposed cascade ESO is explained, theoretically proven, and finally validated in a numerical simulation, let us first recall the standard ESO and highlight its limitations when used in noisy environments. First, a nonlinear dynamical system is represented by the state-space model

$$\begin{cases} \dot{\boldsymbol{x}}(t) = \boldsymbol{A}_n \boldsymbol{x}(t) + \boldsymbol{b}_n (f(\boldsymbol{x}, t) + g(\boldsymbol{x}, t)u(t) + d^*(t)) \\ y(t) = \boldsymbol{c}_n^\top \boldsymbol{x}(t) + w(t) \end{cases}, \quad (1)$$

where $\boldsymbol{x} \triangleq [x_1 \ \dots \ x_n]^\top \in \mathbb{R}^n$ is a system state, $d^* \in \mathbb{R}$ is an external disturbance, $u \in \mathbb{R}$ is a control signal, $y \in \mathbb{R}$ is a system output, $w \in \mathbb{R}$ corresponds to the measurement noise, $g \in \mathbb{R}$ describes the influence of the control signal on the system dynamics, $f \in \mathbb{R}$ represents lumped dynamics of the

K. Łakomy is with the Institute of Automation and Robotics, Poznań University of Technology, Piotrowo 3A, 60-965, Poznań, Poland, e-mail: krzysztof.lakomy92@gmail.com

R. Madonski is with the Energy Electricity Research Center, International Energy College, Jinan University, Zhuhai, Guangdong, 519070 P. R. China, e-mail: rafal.madonski@jnu.edu.cn

controlled plant, while $\boldsymbol{A}_n \triangleq \begin{bmatrix} \boldsymbol{0}^{n-1\times 1} & \boldsymbol{I}^{n-1\times n-1} \\ 0 & \boldsymbol{0}^{1\times n-1} \end{bmatrix} \in \mathbb{R}^{n\times n}$, $\boldsymbol{b}_n \triangleq \begin{bmatrix}\boldsymbol{0}^{n-1\times 1} & 1\end{bmatrix}^\top \in \mathbb{R}^n$, and $\boldsymbol{c}_n \triangleq \begin{bmatrix}1 & \boldsymbol{0}^{n-1\times 1}\end{bmatrix}^\top \in \mathbb{R}^n$.

Assumption 1: System (1) is defined on an arbitrarily large compact domain $\mathcal{D}_x \subset \mathbb{R}^n$, such that $\boldsymbol{x} \in \mathcal{D}_x$.

Assumption 2: Measurement noise is bounded in the sense that there exists a compact set $\mathcal{D}_w \subset \mathbb{R}$, such that $w \in \mathcal{D}_w$.

Assumption 3: External disturbance $d^*(t) \in \mathcal{C}^1$ and $\forall_{t\geq 0}\ d^*(t) < \infty$.

Assumption 4: Fields $g(\boldsymbol{x},t) : \mathcal{D}_x \times \mathbb{R} \to \mathbb{R}$ and $f(\boldsymbol{x},t) : \mathcal{D}_x \times \mathbb{R} \to \mathbb{R}$ are locally Lipschitz, i.e., $g, f \in \mathcal{C}^1$.

Assumption 5: Utilized control law function $u(t)$ is locally Lipschitz, i.e., $u \in \mathcal{C}^1$.

State dynamics, taken from (1), can be rewritten as

$$\begin{cases} \dot{\boldsymbol{x}}(t) = \boldsymbol{A}_n\boldsymbol{x}(t) + \boldsymbol{b}_n\hat{g}u(t) \\ \qquad + \underbrace{\boldsymbol{b}_n(f(\boldsymbol{x},t) + d^*(t) + (g(\boldsymbol{x},t) - \hat{g})u(t))}_{\boldsymbol{b}_n d(\boldsymbol{x},t)} \\ y(t) = \boldsymbol{c}_n^\top \boldsymbol{x}(t) + w(t) \end{cases}, \tag{2}$$

where $d(\boldsymbol{x},t) : \mathcal{D}_x \times \mathbb{R} \to \mathbb{R}$ is the so-called total disturbance, and $\hat{g} \in \mathbb{R}$ is the rough, constant estimate of g. Now let us define the extended state $\boldsymbol{z} \triangleq [\boldsymbol{x}^\top\ d]^\top \in \mathbb{R}^{n+1}$ with the dynamics expressed, according to (2), as

$$\begin{cases} \dot{\boldsymbol{z}}(t) = \boldsymbol{A}_{n+1}\boldsymbol{z}(t) + \boldsymbol{b}_{n+1}\dot{d}(\boldsymbol{z},t) + \boldsymbol{d}_{n+1}\hat{g}u(t) \\ y(t) = \boldsymbol{c}_{n+1}^\top \boldsymbol{z}(t) + w(t) \end{cases}. \tag{3}$$

The standard ESO design, see e.g. [24], is expressed by the dynamics of the extended state estimate $\hat{\boldsymbol{z}} := \boldsymbol{\xi}_1 \in \mathbb{R}^{n+1}$, i.e.,

$$\dot{\boldsymbol{\xi}}_1 = \boldsymbol{A}_{n+1}\boldsymbol{\xi}_1 + \boldsymbol{d}_{n+1}\hat{g}u + \boldsymbol{l}_{1,n+1}(y - \boldsymbol{c}_{n+1}^\top\boldsymbol{\xi}_1), \tag{4}$$

where $\boldsymbol{l}_{1,n+1} \triangleq [\kappa_1\omega_{o1}\ \dots\ \kappa_{n+1}\omega_{o1}^{n+1}]^\top \in \mathbb{R}^{n+1}$ is the observer gain vector dependent on the coefficients $\kappa_i \in \mathbb{R}_+$ for $i \in \{1,...,n+1\}$ and on the parameter $\omega_{o1} \in \mathbb{R}_+$, while $\boldsymbol{d}_{n+1} \triangleq \begin{bmatrix}\boldsymbol{0}^{n-1}\ 1\ 0\end{bmatrix}^\top \in \mathbb{R}^{n+1}$. Observation error can be defined as $\tilde{\boldsymbol{\xi}}_1 \triangleq \boldsymbol{z} - \boldsymbol{\xi}_1 \in \mathbb{R}^{n+1}$, while its dynamics, derived upon (3) and (4), can be expressed as

$$\dot{\tilde{\boldsymbol{\xi}}}_1 = \underbrace{(\boldsymbol{A}_{n+1} - \boldsymbol{l}_{1,n+1}\boldsymbol{c}_{n+1})}_{\boldsymbol{H}_1}\tilde{\boldsymbol{\xi}}_1 + \boldsymbol{b}_{n+1}\dot{d} - \boldsymbol{l}_{1,n+1}w. \tag{5}$$

Remark 1: For the sake of notation conciseness of further analysis, we propose to choose the values of κ_i in a way to obtain matrix $\boldsymbol{H}_1$ with all eigenvalues equal to $-\omega_{o1}$.

Remark 2: Under the Assumptions 1-5, the total disturbance $d \in \mathcal{C}^1$ implying bounded values of its derivative, i.e., guaranteeing $\dot{d} \in \mathcal{D}_{\dot{d}} \subset \mathbb{R}$. The need to ensure bounded values of $\dot{d}$, interpreted as the perturbation of the observation error system (5), is a well-known limitation of the disturbance-observer-based controllers mentioned in [4] and [25].

Now, in order to show the influence of total disturbance and measurement noise on the observation errors for standard ESO, let us first introduce a linear change of coordinates $\tilde{\boldsymbol{\xi}}_1 \triangleq \boldsymbol{\Lambda}_1\boldsymbol{\zeta}_1$, where $\boldsymbol{\Lambda}_1 \triangleq \mathrm{diag}\{\omega_{o1}^{-n}, ..., \omega_{o1}^{-1}, 1\} \in \mathbb{R}^{n+1\times n+1}$ and $\boldsymbol{\zeta}_1 \in \mathbb{R}^{n+1}$, resulting in the transformation of (5) to

$$\begin{aligned} \dot{\boldsymbol{\zeta}}_1 &= \boldsymbol{\Lambda}_1^{-1}\boldsymbol{H}_1\boldsymbol{\Lambda}_1\boldsymbol{\zeta}_1 + \boldsymbol{\Lambda}_1^{-1}\boldsymbol{b}_{n+1}\dot{d} - \boldsymbol{\Lambda}_1^{-1}\boldsymbol{l}_{1,n+1}w \\ &= \omega_{o1}\boldsymbol{H}^*\boldsymbol{\zeta}_1 + \boldsymbol{b}_{n+1}\dot{d} - \boldsymbol{\Lambda}_1^{-1}\boldsymbol{l}_{1,n+1}w, \end{aligned} \tag{6}$$

where

$$\boldsymbol{H}^* = \begin{bmatrix} -\kappa_1 & 1 & \cdots & 0 \\ \vdots & \vdots & \ddots & \vdots \\ -\kappa_n & 0 & \cdots & 1 \\ -\kappa_{n+1} & 0 & \cdots & 0 \end{bmatrix}. \tag{7}$$

We propose a Lyapunov function candidate $V_1 = \boldsymbol{\zeta}_1^\top\boldsymbol{P}\boldsymbol{\zeta}_1$, $V_1 : \mathbb{R}^{n+1} \to \mathbb{R}$ limited by $\lambda_{\min}(\boldsymbol{P})\left\|\boldsymbol{\zeta}_1\right\| \leq V_1 \leq \lambda_{\max}(\boldsymbol{P})\left\|\boldsymbol{\zeta}_1\right\|$, where $\boldsymbol{P} \succ 0$ is the solution of Lyapunov equation

$$\boldsymbol{H}^{*\top}\boldsymbol{P} + \boldsymbol{P}\boldsymbol{H}^* = -\boldsymbol{I}. \tag{8}$$

The derivative of V_1, derived upon (6), can be expressed as

$$\begin{aligned} \dot{V}_1 &= -\omega_{o1}\boldsymbol{\zeta}_1^\top\boldsymbol{\zeta}_1 + 2\boldsymbol{\zeta}_1^\top\boldsymbol{P}\boldsymbol{b}_{n+1}\dot{d} - 2\boldsymbol{\zeta}_1^\top\boldsymbol{P}\boldsymbol{\Lambda}_1^{-1}\boldsymbol{l}_{1,n+1}w \\ &\leq -\omega_{o1}\left\|\boldsymbol{\zeta}_1\right\|^2 + 2\left\|\boldsymbol{P}\right\|\left\|\boldsymbol{\zeta}_1\right\|\left|\dot{d}\right| + 2\left\|\boldsymbol{P}\right\|\kappa_{\max}\omega_{o1}^{n+1}w \end{aligned} \tag{9}$$

for $\kappa_{\max} = \max_j(\kappa_j)$. The derivative of V_1 holds

$$\begin{aligned} &\dot{V}_1 \leq -\omega_{o1}(1-\nu_1)\left\|\boldsymbol{\zeta}_1\right\|^2 \text{ for} \\ &\left\|\boldsymbol{\zeta}_1\right\| \geq \frac{2\left\|\boldsymbol{P}\right\|}{\omega_{o1}\nu_1}|\dot{d}| + \frac{2\left\|\boldsymbol{P}\right\|\kappa_{\max}\omega_{o1}^n}{\nu_1}|w|, \end{aligned} \tag{10}$$

where $\nu_1 \in (0,1)$ is a chosen majorization constant and the conservatively estimated lower bound of $\left\|\boldsymbol{\zeta}_1\right\|$ is a class $\mathcal{K}$ function with respect to arguments $|\dot{d}|$ and $|w|$. According to the result (10), Assumption 2, and Remark 2, we can claim that system (6) is Input-to-State Stable (ISS) and, referring to Th. 4.19 from [26], satisfies

$$\begin{aligned} \limsup_{t\to\infty}\left\|\boldsymbol{\zeta}_1(t)\right\| &\leq \gamma\frac{2\left\|\boldsymbol{P}\right\|}{\omega_{o1}\nu_1}\sup_{t\geq 0}|\dot{d}(t)| \\ &+ \gamma\frac{2\left\|\boldsymbol{P}\right\|\kappa_{\max}\omega_{o1}^n}{\nu_1}\sup_{t\geq 0}|w(t)| \\ &\leq \gamma\frac{2\left\|\boldsymbol{P}\right\|}{\omega_{o1}\nu_1}r_{\dot{d}} + \gamma\frac{2\left\|\boldsymbol{P}\right\|\kappa_{\max}\omega_{o1}^n}{\nu_1}r_w \end{aligned} \tag{11}$$

for $\gamma = \sqrt{\lambda_{\max}(\boldsymbol{P})/\lambda_{\min}(\boldsymbol{P})}$, $\{|\dot{d}| < r_{\dot{d}}\} \subset \mathcal{D}_{\dot{d}}$, and $\{|w| < r_w\} \subset \mathcal{D}_w$. To achieve the minimal asymptotic upper-bound of the transformed observation error $\left\|\boldsymbol{\zeta}_1\right\|$, we need to find a trade-off between the reduction of $|\dot{d}|$ impact with the increasing ω_{o1} values and the influence of $|w|$ amplified by ω_{o1}^n. It is worth noting, that for the nominal case when $\dot{d}(t) \equiv 0$ and $w(t) \equiv 0$, the asymptotic upper bound of $\limsup_{t\to\infty}\left\|\boldsymbol{\zeta}_1\right\| = 0$, implying the asymptotic upper bound of the original observation error vector $\limsup_{t\to\infty}\left\|\tilde{\boldsymbol{\xi}}_1\right\| = 0$. In the case of non-zero values of $|\dot{d}|$ and $w(t) \equiv 0$, $\left\|\boldsymbol{\zeta}_1\right\| \to 0$ as $\omega_{o1} \to \infty$ and $t \to \infty$.

Remark 3: Since in the practical conditions the value of parameter $\omega_{o1} \gg 1$, inequality $\left\|\tilde{\boldsymbol{\xi}}_1\right\| \leq \lambda_{\max}(\boldsymbol{\Lambda}_1)\left\|\boldsymbol{\zeta}_1\right\|$ implies that the asymptotic relation (11) and all of the further comments hold also for the original observation error $\left\|\tilde{\boldsymbol{\xi}}_1\right\|$.

III. Cascade ESO: concept

The concept of ADRC relies on the feedforward cancellation of the total disturbance included in the generic controller

$$u = \hat{g}^{-1}(-\hat{d} + v), \tag{12}$$

where v represents the new virtual control signal, most commonly in the form of a stabilizing feedback controller. Substitution of (12) into the dynamics (2) results in the closed-loop form of the considered system described by

$$\dot{\boldsymbol{x}} = \boldsymbol{A}_n \boldsymbol{x} + \boldsymbol{b}_n \tilde{d} + \boldsymbol{b}_n v, \tag{13}$$

where $\tilde{d} = d - \hat{d} \in \mathbb{R}$ is the residual total disturbance. Let us now assume that the parameter ω_{o1} of the standard ESO, see (4), was set to a relatively low value which only allows a precise following of the first element of extended state, i.e. $\boldsymbol{c}_{n+1}^\top \boldsymbol{z}$, but filters out the measurement noise $w(t)$. Latter elements of the extended state are dependent on the further derivatives of the first one, and usually are more dynamic and have faster transients, thus are not estimated precisely by ESO using chosen ω_{o1}. As a consequence, values of the total disturbance residue $\tilde{d}$ can be substantial causing a possible loss of control precision.

To improve the estimation performance of the extended state obtained with the standard ESO with low ω_{o1}, treated here as a first level in the cascade observer structure, let us introduce the state vector of the second level of the observer $\boldsymbol{\xi}_2 \triangleq [\hat{\xi}_{1,1} \ \widehat{\xi_{1,1}^{(1)}} \ \dots \ \widehat{\xi_{1,1}^{(n-1)}} \ \hat{\tilde{d}}]^\top \in \mathbb{R}^{n+1}$, where $\widehat{\xi_{1,1}^{(i)}}$ for $i \in \{1, .., n-1\}$ is the estimate of i-th derivative of $\xi_{1,1}$, while $\hat{\tilde{d}}$ represents estimated value of a residual total disturbance. The structure of second observer level is designed as

$$\begin{aligned}\dot{\boldsymbol{\xi}}_2(t) &= \boldsymbol{A}_{n+1}\boldsymbol{\xi}_2(t) + \boldsymbol{d}_{n+1} v(t) + \boldsymbol{l}_{2,n+1}\boldsymbol{c}_{n+1}^\top(\boldsymbol{\xi}_1(t) - \boldsymbol{\xi}_2(t)) \\ &\overset{(12)}{=} \boldsymbol{A}_{n+1}\boldsymbol{\xi}_2(t) + \boldsymbol{d}_{n+1}(\hat{g}u(t) + \boldsymbol{b}_{n+1}^\top \boldsymbol{\xi}_1(t)) \\ &\quad + \boldsymbol{l}_{2,n+1}\boldsymbol{c}_{n+1}^\top(\boldsymbol{\xi}_1(t) - \boldsymbol{\xi}_2(t))\end{aligned} \tag{14}$$

where $\boldsymbol{l}_{2,n+1} \triangleq [\kappa_1\omega_{o2} \ \dots \ \kappa_{n+1}\omega_{o2}^{n+1}]^\top \in \mathbb{R}^{n+1}$ and $\omega_{o2} = \alpha\omega_{o1}$, $\alpha > 1$. Note that the equation of the second observer level does not depend on the system output y, thus is not affected by the measurement noise directly. The estimate of total disturbance utilized in (12) should be now taken from the new extended state estimate $\hat{\boldsymbol{z}} := \boldsymbol{\xi}_2 + \boldsymbol{b}_{n+1}\boldsymbol{b}_{n+1}^\top \boldsymbol{\xi}_1$. A block diagram of the proposed observer structure is presented in Fig. 1, where $p = 2$ represents the cascade level in the developed observer structure.

Remark 4: Coefficients κ_i of cascade observer can differ in general between the cascade levels, but for the sake of notation clarity, we assume within this article that they are equal.

Remark 5: The idea of the cascade observer topology is to estimate the total disturbance observation residue resulting from the previous level with the next cascade level of ESO, implying that the observer bandwidth multiplier $\alpha > 1$

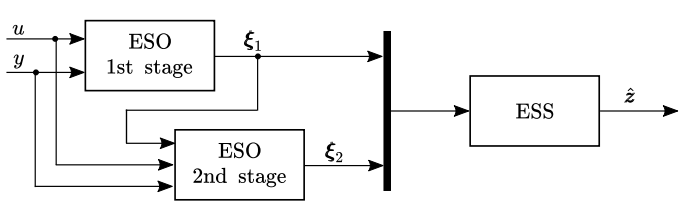

Fig. 1. Cascade ESO for $p = 2$. Extended State Selector (ESS) calculates $\hat{\boldsymbol{z}}$ upon the observer states $\boldsymbol{\xi}_1$, $\boldsymbol{\xi}_2$.

The observation error, associated with the cascade observer with two levels, can be defined as

$$\tilde{\boldsymbol{\xi}}_2 = \boldsymbol{z} - \boldsymbol{\xi}_2 - \boldsymbol{b}_{n+1}\boldsymbol{b}_{n+1}^\top \boldsymbol{\xi}_1, \tag{15}$$

with its dynamics derived upon (14), (4), and (3) as

$$\dot{\tilde{\boldsymbol{\xi}}}_2 = \boldsymbol{H}_2 \tilde{\boldsymbol{\xi}}_2 + \boldsymbol{\Gamma}_{2,1}\tilde{\boldsymbol{\xi}}_1 + \boldsymbol{\delta}_2 w + \boldsymbol{b}_{n+1}\dot{d} \tag{16}$$

for $\boldsymbol{H}_2 = \boldsymbol{A}_{n+1} - \boldsymbol{l}_{2,n+1}\boldsymbol{c}_{n+1}^\top$, $\boldsymbol{\Gamma}_{2,1} = \boldsymbol{l}_{2,n+1}\boldsymbol{c}_{n+1}^\top - \boldsymbol{b}_{n+1}\boldsymbol{b}_{n+1}^\top \boldsymbol{l}_{1,n+1}\boldsymbol{c}_{n+1}^\top$ and $\boldsymbol{\delta}_2 = -\boldsymbol{b}_{n+1}\boldsymbol{b}_{n+1}^\top \boldsymbol{l}_{1,n+1}\boldsymbol{c}_{n+1}^\top$.

Following the reasoning presented in Sect. II for standard ESO, we now prove that the observation error $\tilde{\boldsymbol{\xi}}_2$ is bounded, despite a perturbing impact of total disturbance and measurement noise. Let us introduce a linear change of coordinates $\tilde{\boldsymbol{\xi}}_2 \triangleq \boldsymbol{\Lambda}_2\boldsymbol{\zeta}_2$ for $\boldsymbol{\Lambda}_2 \triangleq \mathrm{diag}\{\omega_{o2}^{-n}, ..., \omega_{o2}^{-1}, 1\} \in \mathbb{R}^{n+1\times n+1}$, and $\boldsymbol{\zeta}_2 \in \mathbb{R}^{n+1}$. The dynamics of $\boldsymbol{\zeta}_2$ is described by

$$\begin{aligned}\dot{\boldsymbol{\zeta}}_2 &= \boldsymbol{\Lambda}_2^{-1}\boldsymbol{H}_2\boldsymbol{\Lambda}_2\boldsymbol{\zeta}_2 + \boldsymbol{\Lambda}_2^{-1}\boldsymbol{\Gamma}_{2,1}\boldsymbol{\Lambda}_1\boldsymbol{\zeta}_1 + \boldsymbol{\Lambda}_2^{-1}\boldsymbol{\delta}_2 w + \boldsymbol{\Lambda}_2^{-1}\boldsymbol{b}_{n+1}\dot{d} \\ &= \omega_{o2}\boldsymbol{H}^*\boldsymbol{\zeta}_2 + \boldsymbol{\Lambda}_2^{-1}\boldsymbol{\Gamma}_{2,1}\boldsymbol{\Lambda}_1\boldsymbol{\zeta}_1 + \boldsymbol{\Lambda}_2^{-1}\boldsymbol{\delta}_2 w + \boldsymbol{b}_{n+1}\dot{d}\end{aligned} \tag{17}$$

for matrix $\boldsymbol{H}^*$ taken from (7). Let us introduce a Lyapunov function candidate in the form $V_2 \triangleq \boldsymbol{\zeta}_2^\top \boldsymbol{P}\boldsymbol{\zeta}_2$, $V_2 : \mathbb{R}^{n+1} \to \mathbb{R}$ limited by $\lambda_{\min}(\boldsymbol{P})\|\boldsymbol{\zeta}_2\| \le V_2 \le \lambda_{\max}(\boldsymbol{P})\|\boldsymbol{\zeta}_2\|$, where $\boldsymbol{P}$ is a solution of the Lyapunov equation (8). The derivative of V_2, calculated with (17), has the form

$$\begin{aligned}\dot{V}_2 &= -\omega_{o2}\boldsymbol{\zeta}_2^\top\boldsymbol{\zeta}_2 + 2\boldsymbol{\zeta}_2^\top\boldsymbol{P}\boldsymbol{\Lambda}_2^{-1}\boldsymbol{\Gamma}_{2,1}\boldsymbol{\Lambda}_1\boldsymbol{\zeta}_1 + 2\boldsymbol{\zeta}_2^\top\boldsymbol{P}\boldsymbol{\Lambda}_2^{-1}\boldsymbol{\delta}_2 w \\ &\quad + 2\boldsymbol{\zeta}_2^\top\boldsymbol{P}\boldsymbol{b}_{n+1}\dot{d} \\ &\le -\omega_{o2}\|\boldsymbol{\zeta}_2\|^2 + 2\kappa_{\max}\alpha^{n+1}\omega_{o1}\|\boldsymbol{P}\|\|\boldsymbol{\zeta}_1\|\|\boldsymbol{\zeta}_2\| \\ &\quad + 2\omega_{o1}^{n+1}\|\boldsymbol{P}\||w|\|\boldsymbol{\zeta}_2\| + 2\|\boldsymbol{P}\||\dot{d}|\|\boldsymbol{\zeta}_2\|,\end{aligned} \tag{18}$$

which holds

$$\begin{aligned}&\dot{V}_2 \le -\omega_{o2}(1-\nu_2)\|\boldsymbol{\zeta}_2\|^2 \ \text{ for} \\ &\|\boldsymbol{\zeta}_2\| \ge \frac{2\kappa_{\max}\alpha^n\|\boldsymbol{P}\|}{\nu_2}\|\boldsymbol{\zeta}_1\| + \frac{2\omega_{o1}^n\|\boldsymbol{P}\|}{\alpha\nu_2}|w| + \frac{2\|\boldsymbol{P}\|}{\omega_{o2}\nu_2}|\dot{d}|,\end{aligned} \tag{19}$$

where $\nu_2 \in (0,1)$ is a chosen majorization constant and the conservatively estimated lower bound of the transformed observation error $\|\boldsymbol{\zeta}_2\|$ is a class $\mathcal{K}$ function with respect to the arguments $\|\boldsymbol{\zeta}_1\|$, $|w|$, and $|\dot{d}|$. According to the result (19), the system (17) is ISS and satisfies the asymptotic relation

$$\begin{aligned}\limsup_{t\to 0}\|\boldsymbol{\zeta}_2(t)\| &\le \gamma\frac{2\kappa_{\max}\alpha^n\|\boldsymbol{P}\|}{\nu_2}\limsup_{t\to\infty}\|\boldsymbol{\zeta}_1(t)\| \\ &\quad + \gamma\frac{2\omega_{o1}^n\|\boldsymbol{P}\|}{\alpha\nu_2}\sup_{t\ge 0}|w(t)| + \frac{2\|\boldsymbol{P}\|}{\omega_{o2}\nu_2}\sup_{t\ge 0}|\dot{d}(t)| \\ &\overset{(11)}{\le} \gamma\left[\frac{2\omega_{o1}^n\|\boldsymbol{P}\|}{\alpha\nu_2} + \frac{4\kappa_{\max}^2\alpha^n\omega_{o1}^n\|\boldsymbol{P}\|^2}{\nu_2\nu_1}\right]r_w \\ &\quad + \gamma\left[\frac{2\|\boldsymbol{P}\|}{\omega_{o2}\nu_2} + \frac{4\kappa_{\max}\alpha^n\|\boldsymbol{P}\|^2}{\nu_2\nu_1\omega_{o1}}\right]r_{\dot{d}},\end{aligned} \tag{20}$$

for γ, $r_{\dot{d}}$, r_w having the same values as the ones from (11). Summarizing, the transformed observation error is bounded in general, $\|\boldsymbol{\zeta}_2\| \to 0$ as $\omega_{o1} \to \infty$ and $t \to \infty$ when $w \equiv 0$, and $\limsup_{t\to\infty}\|\boldsymbol{\zeta}_2(t)\| = 0$ when both $w \equiv 0$ and $\dot{d} \equiv 0$. Similarly to the issue described in Remark 3 for the single-stage observer, the original observation error for

the second-level cascade observer ($p = 2$) satisfies $\left\|\tilde{\boldsymbol{\xi}}_2\right\| \leq \lambda_{\max}(\boldsymbol{\Lambda}_2)\left\|\boldsymbol{\zeta}_2\right\| \leq \left\|\boldsymbol{\zeta}_2\right\|$ and thus holds limit (20).

IV. Cascade ESO: general design

In the general case, we may continue the procedure of estimating residual observation errors by increasing the level of observer cascade to the arbitrarily chosen value $p = k$ such that $k \in \mathbb{Z}$ and $k \geq 2$. The cascade observer with i levels can be written down as

$$\begin{aligned}\dot{\boldsymbol{\xi}}_1(t) &= \boldsymbol{A}_{n+1}\boldsymbol{\xi}_1(t) + \boldsymbol{d}_{n+1}\hat{g}u(t) + \boldsymbol{l}_{1,n+1}(y(t) - \boldsymbol{c}_{n+1}^\top\boldsymbol{\xi}_1(t))\\ \dot{\boldsymbol{\xi}}_i(t) &= \boldsymbol{A}_{n+1}\boldsymbol{\xi}_i(t) + \boldsymbol{d}_{n+1}\left(\hat{g}u(t) + \boldsymbol{b}_{n+1}^\top\sum_{j=1}^{i-1}\boldsymbol{\xi}_j(t)\right)\\ &\quad + \boldsymbol{l}_{i,n+1}\boldsymbol{c}_{n+1}^\top(\boldsymbol{\xi}_{i-1}(t) - \boldsymbol{\xi}_i(t))\end{aligned} \tag{21}$$

for $i \in \{2, ..., p\}$ and $\omega_{oi} = \alpha\omega_{oi-1}$ for $\alpha > 1$. The estimate of total disturbance implemented in (12) can be taken from the new extended state estimate expressed as $\hat{\boldsymbol{z}} := \boldsymbol{\xi}_i + \boldsymbol{b}_{n+1}\boldsymbol{b}_{n+1}^\top\sum_{j=1}^{i-1}\boldsymbol{\xi}_j$.

The observation error for the i-level cascade ESO is

$$\tilde{\boldsymbol{\xi}}_i \triangleq \boldsymbol{z} - \boldsymbol{\xi}_i - \boldsymbol{b}_{n+1}\boldsymbol{b}_{n+1}^\top\sum_{j=1}^{i-1}\boldsymbol{\xi}_j \tag{22}$$

with the dynamics expressed (after some algebraic manipulations made according to (3), and (21)) as

$$\dot{\tilde{\boldsymbol{\xi}}}_i = \boldsymbol{H}_i\tilde{\boldsymbol{\xi}}_i + \boldsymbol{\Gamma}_{i,i-1}\tilde{\boldsymbol{\xi}}_{i-1} + \boldsymbol{b}_{n+1}^\top\dot{d} + \sum_{j=1}^{i-2}\boldsymbol{\Gamma}_{i,j}\tilde{\boldsymbol{\xi}}_j + \boldsymbol{\delta}_i w \tag{23}$$

for $\boldsymbol{H}_i = \boldsymbol{A}_{n+1} - \boldsymbol{l}_{i,n+1}\boldsymbol{c}_{n+1}^\top$, $\boldsymbol{\Gamma}_{i,i-1} = \boldsymbol{l}_{i,n+1}\boldsymbol{c}_{n+1}^\top - \boldsymbol{b}_{n+1}\boldsymbol{b}_{n+1}^\top\boldsymbol{l}_{i-1,n+1}\boldsymbol{c}_{n+1}^\top$, $\boldsymbol{\Gamma}_{i,j} = -\boldsymbol{b}_{n+1}\boldsymbol{b}_{n+1}^\top\boldsymbol{l}_{j,n+1}\boldsymbol{c}_{n+1}^\top$, and $\boldsymbol{\delta}_i = -\boldsymbol{b}_{n+1}\boldsymbol{b}_{n+1}^\top\boldsymbol{l}_{1,n+1}\boldsymbol{c}_{n+1}^\top$. Using the linear change of coordinates $\boldsymbol{\xi}_i = \boldsymbol{\Lambda}_i\boldsymbol{\zeta}_i$ for $\boldsymbol{\Lambda}_i \triangleq \mathrm{diag}\{-\omega_{o1}^{-n}, ..., -\omega_{o1}^{-1}, 1\} \in \mathbb{R}^{n+1\times n+1}$ and $\boldsymbol{\zeta}_i \in \mathbb{R}^{n+1}$, we may rewrite the observation error dynamics concerning i-th level structure as

$$\begin{aligned}\dot{\boldsymbol{\zeta}}_i &= \underbrace{\boldsymbol{\Lambda}_i^{-1}\boldsymbol{H}_i\boldsymbol{\Lambda}_i}_{\omega_{oi}\boldsymbol{H}^*}\boldsymbol{\zeta}_i + \boldsymbol{\Lambda}_i^{-1}\boldsymbol{\Gamma}_{i,i-1}\boldsymbol{\Lambda}_{i-1}\boldsymbol{\zeta}_{i-1} + \boldsymbol{\Lambda}_i^{-1}\boldsymbol{b}_{n+1}\dot{d}\\ &\quad + \boldsymbol{\Lambda}_i^{-1}\sum_{j=1}^{i-2}\boldsymbol{\Gamma}_{i,j}\boldsymbol{\Lambda}_j\boldsymbol{\zeta}_j + \boldsymbol{\Lambda}_i^{-1}\boldsymbol{\delta}_i w.\end{aligned} \tag{24}$$

To prove the boundedness of observation errors in the general case of cascade ESO, let us propose a Lyapunov function candidate defined as $V_i \triangleq \boldsymbol{\zeta}_i^\top\boldsymbol{P}\boldsymbol{\zeta}_i$, $V_i : \mathbb{R}^{n+1} \to \mathbb{R}$ and bounded by $\lambda_{\min}(\boldsymbol{P})\left\|\boldsymbol{\zeta}_2\right\| \leq V_2 \leq \lambda_{\max}(\boldsymbol{P})\left\|\boldsymbol{\zeta}_2\right\|$, where $\boldsymbol{P}$ is a solution of an algebraic Lyapunov equation (8). The derivative of V_i is calculated upon (24) and takes the form

$$\begin{aligned}\dot{V}_i &= -\omega_{oi}\boldsymbol{\zeta}_i^\top\boldsymbol{\zeta}_i + 2\boldsymbol{\zeta}_i^\top\boldsymbol{P}\boldsymbol{\Lambda}_i^{-1}\boldsymbol{\delta}_i w + 2\boldsymbol{\zeta}_i^\top\boldsymbol{P}\boldsymbol{\Lambda}_i^{-1}\boldsymbol{b}_{n+1}\dot{d}\\ &\quad + 2\boldsymbol{\zeta}_i^\top\boldsymbol{P}\boldsymbol{\Lambda}_i^{-1}\boldsymbol{\Gamma}_{i,i-1}\boldsymbol{\Lambda}_{i-1}\boldsymbol{\zeta}_{i-1} + 2\boldsymbol{\zeta}_i^\top\boldsymbol{P}\boldsymbol{\Lambda}_i^{-1}\sum_{j=1}^{i-2}\boldsymbol{\Gamma}_{i,j}\boldsymbol{\Lambda}_j\boldsymbol{\zeta}_j\\ &\leq -\omega_{oi}\left\|\boldsymbol{\zeta}_i\right\|^2 + 2\left\|\boldsymbol{P}\right\|\left\|\boldsymbol{\zeta}_i\right\|\omega_{o1}^{n+1}|w| + 2\left\|\boldsymbol{P}\right\|\left\|\boldsymbol{\zeta}_i\right\||\dot{d}|\\ &\quad + 2\frac{\kappa_{\max}\omega_{oi}^{n+1}}{\omega_{oi-1}^n}\left\|\boldsymbol{P}\right\|\left\|\boldsymbol{\zeta}_{i-1}\right\|\left\|\boldsymbol{\zeta}_i\right\| + 2\left\|\boldsymbol{P}\right\|\left\|\boldsymbol{\zeta}_i\right\|\sum_{j=1}^{i-2}\omega_{oj}\left\|\boldsymbol{\zeta}_j\right\|\end{aligned} \tag{25}$$

that holds

$$\begin{aligned}\dot{V}_i &\leq -\omega_{oi}(1-\nu_i)\left\|\boldsymbol{\zeta}_i\right\|^2 \text{ for}\\ \left\|\boldsymbol{\zeta}_i\right\| &\geq \frac{2\kappa_{\max}\omega_{oi}^n\left\|\boldsymbol{P}\right\|}{\nu_i\omega_{oi-1}^n}\left\|\boldsymbol{\zeta}_{i-1}\right\|\\ &\quad + \frac{2\left\|\boldsymbol{P}\right\|}{\nu_i\omega_{oi}}\sum_{j=1}^{i-2}\omega_{oj}\left\|\boldsymbol{\zeta}_j\right\| + \frac{2\left\|\boldsymbol{P}\right\|}{\nu_i\omega_{oi}}|\dot{d}| + \frac{2\left\|\boldsymbol{P}\right\|\omega_{o1}^{n+1}}{\nu_i\omega_{oi}}|w|\\ &= \frac{2\kappa_{\max}\alpha^n\left\|\boldsymbol{P}\right\|}{\nu_i}\left\|\boldsymbol{\zeta}_{i-1}\right\| + \frac{2\left\|\boldsymbol{P}\right\|}{\nu_i}\sum_{j=1}^{i-2}\frac{1}{\alpha^{i-j}}\left\|\boldsymbol{\zeta}_j\right\|\\ &\quad + \frac{2\left\|\boldsymbol{P}\right\|}{\nu_i\alpha^{i-1}\omega_{o1}}|\dot{d}| + \frac{2\left\|\boldsymbol{P}\right\|\omega_{o1}^n}{\nu_i\alpha^{i-1}}|w|.\end{aligned} \tag{26}$$

According to the ISS procedure, steady-state values of the transformed observation error are limited by

$$\begin{aligned}&\limsup_{t\to\infty}\left\|\boldsymbol{\zeta}_i(t)\right\| \leq \gamma\frac{2\kappa_{\max}\alpha^n\left\|\boldsymbol{P}\right\|}{\nu_i}\limsup_{t\to\infty}\left\|\boldsymbol{\zeta}_{i-1}(t)\right\|\\ &+ \gamma\frac{2\left\|\boldsymbol{P}\right\|}{\nu_i}\sum_{j=1}^{i-2}\frac{1}{\alpha^{i-j}}\limsup_{t\to\infty}\left\|\boldsymbol{\zeta}_j(t)\right\|\\ &+ \gamma\frac{2\left\|\boldsymbol{P}\right\|}{\nu_i\alpha^{i-1}\omega_{o1}}\sup_{t\geq 0}|\dot{d}(t)| + \gamma\frac{2\left\|\boldsymbol{P}\right\|\omega_{o1}^{n-1}}{\nu_i\alpha^{i-1}}\sup_{t\geq 0}|w(t)|,\end{aligned} \tag{27}$$

where γ is taken from (11). Due to the recursive character of the obtained asymptotic relation and the result (11), we may also write that $\limsup_{t\to\infty}\left\|\boldsymbol{\zeta}_i\right\| \leq c_1 r_{\dot{d}} + c_2 r_w$ for some positive constants c_1, c_2 dependent on the parameters ω_{o1} and α. As it was presented for previously described observer structures, transformed observation error is generally bounded, $\left\|\boldsymbol{\zeta}_i\right\| \to 0$ as $\omega_{o1} \to \infty$ and $t \to \infty$ when $w(t) \equiv 0$, and $\limsup_{t\to\infty}\left\|\boldsymbol{\zeta}_i(t)\right\| = 0$ when both $w(t) \equiv 0$ and $\dot{d}(t) \equiv 0$. Similarly to the issue described in Remark 3 for the single-level observer structure, the original observation error for the i-level cascade observer $\left\|\tilde{\boldsymbol{\xi}}_i\right\| \leq \lambda_{\max}(\boldsymbol{\Lambda}_i)\left\|\boldsymbol{\zeta}_i\right\| \leq \left\|\boldsymbol{\zeta}_i\right\|$ and thus holds limit (27).

V. Numerical verification

A. Methodology

In order to evaluate the effectiveness of the proposed cascade ESO-based ADRC design (Sect. III and IV) in terms of control objective realization and measurement noise attenuation, its results are quantitatively compared with the results from a standard, single ESO-based ADRC design (Sect. II). For the purpose of this case study, a following second order system in form of (1) is considered:

$$\begin{cases}\dot{\boldsymbol{x}}(t) = \boldsymbol{A}_2\boldsymbol{x}(t) + \boldsymbol{b}_2(f(\boldsymbol{x}) + g\cdot u(t) + d^*(t))\\ y(t) = \boldsymbol{c}_2^\top\boldsymbol{x}(t) + w(t)\end{cases}, \tag{28}$$

with $\boldsymbol{x} = \left[\begin{smallmatrix}x_1\\x_2\end{smallmatrix}\right]$, $f(\boldsymbol{x}) = -x_1 - 2x_2$, and $g = 1$. The core linear dynamics of (28) is affected (starting at $t = 3.5$s) by an external, nonlinear disturbance $d^*(t) = 5\sin(9t)$. The control objective is to make the output $y(t)$ track a desired trajectory $y_d(t) \in \mathbb{R}$ in the presence of measurement noise $w(t)$ and despite the influence of $d^*(t)$. Signal $y_d(t)$ here is a step function, additionally filtered by a stable dynamics $G_f(s) = 1/(0.1s+1)^5$ to minimize the observer peaking.

TABLE I
CONTROL DESIGNS USED IN THE COMPARISON.

Observer type	Observer bandwidth
Standard ESO p=1	$\omega_{o1} = 400$
Proposed ESO p=2	$\omega_{o1} = 75$, $\omega_{o2} = 2\omega_{o1}$
Proposed ESO p=3	$\omega_{o1} = 40$, $\omega_{o2} = 2\omega_{o1}$, $\omega_{o3} = 2\omega_{o2}$

TABLE II
ASSESSMENT BASED ON SELECTED INTEGRAL QUALITY CRITERIA.

Test	Observer type	Criterion		
		$10^3 \int \lvert e(t)\rvert dt$	$\int \lvert u(t)\rvert dt$	$\int \lvert \tilde{z}_3(t)\rvert dt$
SimA	Standard ESO p=1	9.963	46.949	**0.521**
	Proposed ESO p=2	6.297	50.096	**0.520**
	Proposed ESO p=3	4.355	49.013	**0.521**
SimB	Standard ESO p=1	10.031	98.922	10.092
	Proposed ESO p=2	6.615	53.563	3.120
	Proposed ESO p=3	4.625	51.540	2.881

The control action u is defined the same for all tested cases as in (12), with $v = \ddot{y}_d + 4(\dot{y}_d - \xi_{p,2}) + 4(y_d - \xi_{p,1})$. To keep the conciseness of notation, we treat the standard ESO as the case with $p = 1$. Two comparison tests are performed.

SimA: trajectory tracking without measurement noise. In order to establish a fair base for further comparison in the presence of measurement noise, similar performance between the tested control designs is achieved first in the idealized, noise-less conditions ($w(t) = 0$). Since total disturbance estimation is the key element in any ADRC approach, the focus here is on providing similar reconstruction quality of $\hat{d}$ in terms of minimizing integral criterion $\int |\tilde{z}_3(t)|dt$, with $\tilde{z}_3(t)$ being the total disturbance observation error taken from $\tilde{\boldsymbol{z}} = [\tilde{z}_1 \;\; \tilde{z}_2 \;\; \tilde{z}_3]^\top \triangleq \tilde{\boldsymbol{\xi}}_p$. Since the tested control algorithms do not share similar observer structure, nor have the same number of tuning parameters, it is arbitrarily decided to use a tuning methodology of single observer bandwidth parameterization from [24], which is based on a standard pole-placement procedure (cf. *Remark 1*). The heuristically selected observer bandwidths from Table I provide the similar total disturbance reconstruction quality among the tested algorithms, as confirmed by Table II. Two integral criteria are additionally introduced to evaluate overall tracking accuracy ($10^3 \int |e(t)|dt$) and energy usage ($\int |u(t)|dt$).

SimB: trajectory tracking with measurement noise. This time, a more realistic scenario is considered in which the output measurement noise is present (i.e. $w(t) \neq 0$), hence the only change w.r.t. test *SimA* is the introduction of the band-limited white noise $w(t)$ with power $1e^{-10}$.

B. Results and discussion

The results of *SimA* are gathered in Fig. 2. The selected observer bandwidths provide visually comparable results of total disturbance estimation error ($\tilde{z}_3(t)$) and energy consumption ($u(t)$) in all tested control designs, even though both cascade ESO-based designs have significantly lower observer bandwidths than standard approach. The proposed cascade ESO structures also improve the tracking quality ($e(t)$) despite having lower observer bandwidths. The observation error $\tilde{z}_1(t)$ differs among tested techniques noticeably, however, it is expected result since in the cascade observer design, the importance of output signal estimation is being shifted and favors total disturbance estimation instead. It is done deliberately and has practical justification as it is often the case that the output signal is available directly through measurement, hence its close estimation would be redundant.

The results of *SimB* are gathered in Fig. 3. The cascade ESO provides improvement in noise attenuation over standard ESO, especially in the quality of total disturbance reconstruction and, consequently, in the control signal profile (Table II). With the extra layer of cascade ($p = 3$), the amplitude of noise is further reduced. It is not surprising since with the increase of cascade level, lower observer bandwidths can be selected for estimating signals contaminated with high-frequency noise (hence noise is not over-amplified). At the same time, high observer bandwidths can be selected for estimating signals which are affected by the noise to a smaller extent, hence high tracking capabilities can be retained.

Additionally, Fig. 4 shows relative quality of total disturbance estimation (understood as minimizing criterion $\int |\tilde{z}_3(t)|dt$) between standard and proposed ESO-based designs in tests *SimA* (left) and *SimB* (right). In both instances, the blue color represents area where the total disturbance is estimated more precisely using cascade ESO ($p = 2$) with $\alpha = 2$, while the red color represents area where the standard ESO provides better estimation. The dashed line in the left-hand side figure connects points with equal values of estimation precision, i.e., cases having similar convergence speed of observation error (cf. Fig. 2). When the same dashed line is plotted in the right-hand side figure, it is surrounded by blue area for high observer bandwidths (ω_{o1}) of standard ESO. This confirms numerically that the use of cascade ESO is justified when high observer gains are demanded, as it can improve the estimation precision (connected with noise attenuation) for similar convergence speed.

From the obtained results, one can deduce that the compromise between speed/accuracy of state reconstruction and noise amplification is still present, however, with the cascade ESO one gains extra degree of freedom in designing high-bandwidth observers while minimizing the amplification of output noise. This reveals great practical potential of the proposed method in high-performance control of systems subjected to non-negligible measurement noise. The potential drawbacks of the proposed cascade ESO-based design (like extra tuning parameters, lack of a systematic method of cascade level selection and cascade ESO tuning) as well as increased computational complexity need to be further investigated. Future work includes comprehensive comparison (both quantitative and qualitative) with other noise attenuation techniques dedicated to high-gain observers (see Introduction) as well as experimental validation.

REFERENCES

[1] E. Sariyildiz, R. Oboe, and K. Ohnishi, "Disturbance observer-based robust control and its applications: 35th anniversary overview," *IEEE Transactions on Industrial Electronics*, vol. 67, no. 3, pp. 2042–2053, 2020.

[2] Z. Gao, "On the centrality of disturbance rejection in automatic control," *ISA Transactions*, vol. 53, no. 4, pp. 850–857, 2014.

[3] J. Han, "From PID to Active Disturbance Rejection Control," *IEEE Transactions on Industrial Electronics*, vol. 56, no. 3, pp. 900–906, 2009.

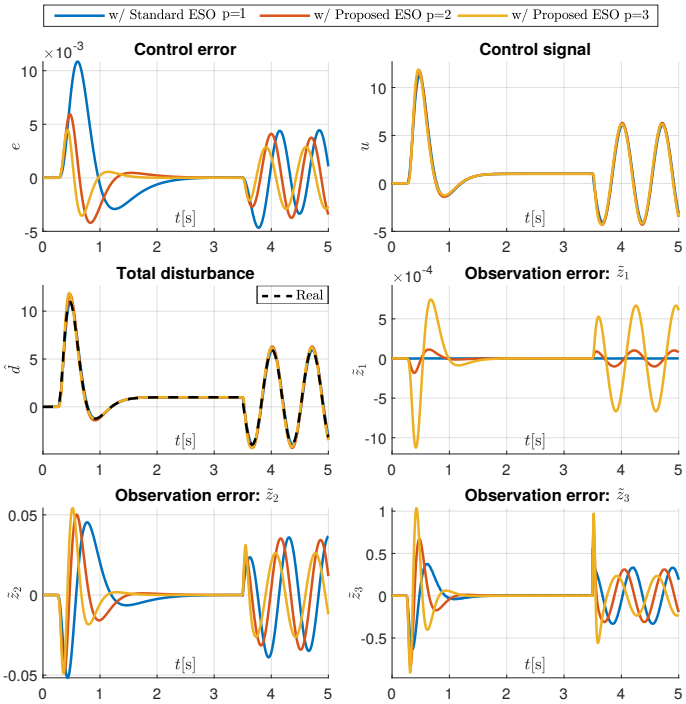

Fig. 2. Results of test *SimA* (i.e. without measurement noise: $w(t) = 0$).

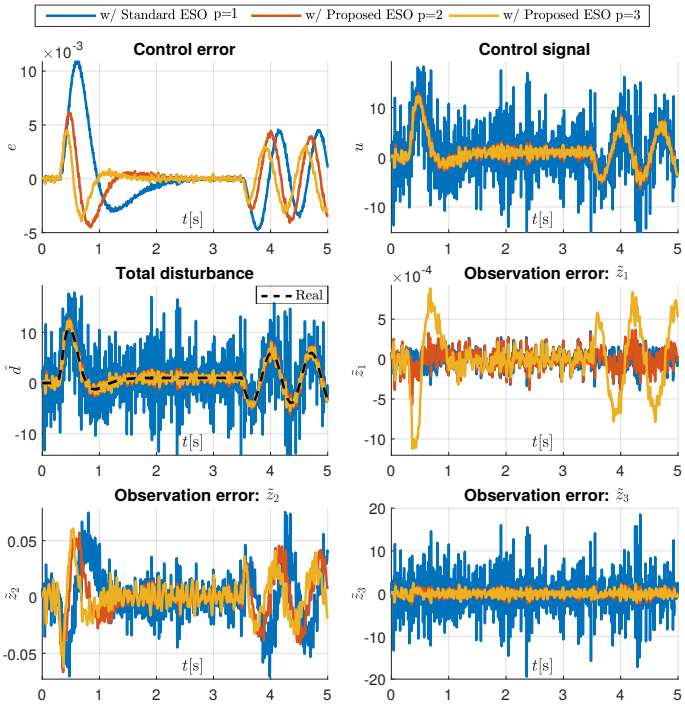

Fig. 3. Results of test *SimB* (i.e. with measurement noise: $w(t) \neq 0$).

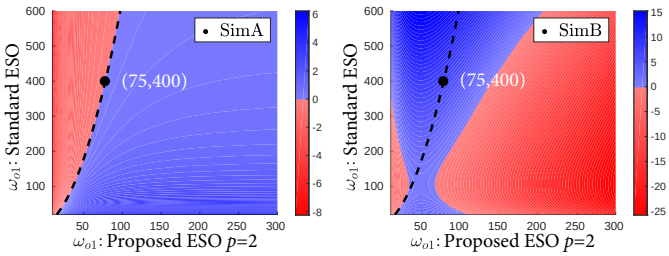

Fig. 4. Difference between $\int |\tilde{z}_3(t)|dt$ values obtained for the standard and the proposed cascade ESO ($p = 2$) in tests *SimA* ($w(t) = 0$; left figure) and *SimB* ($w(t) \neq 0$; right figure). Point (75,400) represents the specific pair of observer bandwidths used in both tests (see Table I).

[4] S. Chen and Z. Chen, "On active disturbance rejection control for a class of uncertain systems with measurement uncertainty (early access)," *IEEE Transactions on Industrial Electronics*, pp. 1–1, 2020.

[5] T. Liu, S. Hao, D. Li, W. Chen, and Q. Wang, "Predictor-based disturbance rejection control for sampled systems with input delay," *IEEE Transactions on Control Systems Technology*, vol. 27, no. 2, pp. 772–780, 2019.

[6] H. Sira-Ramírez, E. W. Zurita-Bustamante, and C. Huang, "Equivalence among flat filters, dirty derivative-based PID controllers, ADRC, and integral reconstructor-based sliding mode control (early access)," *IEEE Transactions on Control Systems Technology*, pp. 1–15, 2019.

[7] M. M. Michałek, K. Łakomy, and W. Adamski, "Robust output-feedback cascaded tracking controller for spatial motion of anisotropically-actuated vehicles," *Aerospace Science and Technology*, vol. 92, pp. 915 – 929, 2019. [Online]. Available: http://www.sciencedirect.com/science/article/pii/S1270963818314354

[8] H. K. Khalil and L. Praly, "High-gain observers in nonlinear feedback control," *International Journal of Robust and Nonlinear Control*, vol. 24, no. 6, pp. 993–1015, 2014. [Online]. Available: https://onlinelibrary.wiley.com/doi/abs/10.1002/rnc.3051

[9] A. A. Prasov and H. K. Khalil, "A nonlinear high-gain observer for systems with measurement noise in a feedback control framework," *IEEE Transactions on Automatic Control*, vol. 58, no. 3, pp. 569–580, 2013.

[10] J. H. Ahrens and H. K. Khalil, "High-gain observers in the presence of measurement noise: a switched-gain approach," *Automatica*, vol. 45, no. 4, pp. 936–943, 2009.

[11] R. G. Sanfelice and L. Praly, "On the performance of high-gain observers with gain adaptation under measurement noise," *Automatica*, vol. 47, no. 10, pp. 2165–2176, 2011.

[12] S. Battilotti, "Robust observer design under measurement noise with gain adaptation and saturated estimates," *Automatica*, vol. 81, pp. 75–86, 2017.

[13] N. Boizot, E. Buswelle, and J. P. Gauthier, "An adaptive high-gain observer for nonlinear systems," *Automatica*, vol. 46, p. 1483–1488, 2010.

[14] D. Astolfi, R. Postoyan, and D. Nesic, "Uniting local and global observers for the state estimation of nonlinear continuous-time systems," in *Proc. Conference on Decision and Control*, 2017, pp. 3039–3044.

[15] A. Zemouche, F. Zhang, F. Mazenc, and R. Rajamani, "High-gain nonlinear observer with lower tuning parameter," *IEEE Transactions on Automatic Control*, vol. 64, no. 8, pp. 3194–3209, 2019.

[16] W. Xue, X. Zhang, L. Sun, and H. Fang, "Extended state filter based disturbance and uncertainty mitigation for nonlinear uncertain systems with application to fuel cell temperature control (early access)," *IEEE Transactions on Industrial Electronics*, pp. 1–1, 2020.

[17] L. Wang, D. Astolfi, L. Marconi, and H. Su, "High-gain observers with limited gain power for systems with observability canonical form," *Automatica*, vol. 75, pp. 16–23, 2017.

[18] H. K. Khalil, "Cascade high-gain observers in output feedback control," *Automatica*, vol. 80, pp. 110–118, 2017.

[19] K. K. Busawon and P. Kabore, "Disturbance attenuation using proportional integral observers," *International Journal of Control*, vol. 74, no. 6, pp. 618–627, 2001.

[20] L. Z. D. Astolfi, A. Alessandri, "Stubborn ISS redesign for nonlinear high-gain observers," in *Proc. IFAC World Congress*, 2017.

[21] G. Herbst, "Practical active disturbance rejection control: bumpless transfer, rate limitation, and incremental algorithm," *IEEE Transactions on Industrial Electronics*, vol. 63, no. 3, pp. 1754–1762, 2016.

[22] D. Astolfi, M. Jungers, and L. Zaccarian, "Output injection filtering redesign in high-gain observers," in *Proc. European Control Conference*, 2018, pp. 1957–1962.

[23] H. K. Khalil and S. Priess, "Analysis of the use of low-pass filters with high-gain observers," *IFAC-PapersOnLine*, vol. 49, no. 18, pp. 488–492, 2016, IFAC Symposium on Nonlinear Control Systems.

[24] Z. Gao, "Scaling and bandwidth-parameterization based controller tuning," in *Proc. American Control Conference*, vol. 6, 2003, pp. 4989–4996.

[25] D. Astolfi and L. Marconi, "A high-gain nonlinear observer with limited gain power," *IEEE Transactions on Automatic Control*, vol. 60, no. 11, pp. 3059–3064, 2015.

[26] H. K. Khalil, *Nonlinear systems, 3rd edition*. New Jersey: Prentice Hall, 2002.